34th Annual International Conference of the IEEE EMBS
San Diego, California USA, 28 August - 1 September, 2012

Computational Model of Electrical Stimulation of a Retinal Ganglion Cell with Hexagonally Arranged Electrodes

Miganoosh Abramian, *Member IEEE*, Nigel H. Lovell, *Fellow IEEE*, John W. Morley, Gregg J. Suaning, *Member IEEE*, and Socrates Dokos, *Member IEEE*

***Abstract*—In retinal prosthetic devices an electrode array is used for electrical stimulation of retinal neurons to induce phosphene perception. The shape and size of the evoked phosphenes are in part dependent on the spatial patterns of retinal activation. In this study, a computational model of a cat beta retinal ganglion cell (RGC) excitation following simulated electrical stimulation was investigated. Seven epiretinal disk electrodes with hexagonal configuration (Hex electrodes) were used. 100 µs/phase anodic-first biphasic pulses were injected at the center electrode and one sixth of the total current was returned at each surround electrode. The aim was to obtain a spatial threshold map of the RGC excitation. We found that the spatial threshold pattern was highly dominated by axonal excitation. With 50 µm Hex electrodes, relative thresholds for activation of the distal axon was almost the same as that for excitation of the axonal trigger segment (high sodium channel density region), causing an elongated activation pattern. The model presented in this study can be used to investigate the extent to which spatial RGC activation patterns are influenced by cell and stimulus parameters.**

I. Introduction

Retinal prosthetic devices are being developed worldwide in an attempt to provide functional vision to those blinded by outer retinal degenerative diseases. Although there have been significant advances in the field and recent clinical trials have shown promising results, a prosthetic device that can elicit phosphene images with high quality and resolution is still a long way off (for a review see [1]). Elongated, rather than round, phosphenes and complex phosphene patterns following multi-electrode stimulation have been reported as some of the factors contributing to the poor quality of the percepts [2, 3].

To achieve useful vision, a large number of stimulating electrodes [4] and high frequency stimulation [5] are required, which impose the need to use parallel stimulation. In parallel stimulation mode, electrode cross-talk is a major challenge, which occurs due to current diversion between stimulating electrodes [6]. The retinal prosthetic device being developed by our research group has a hexagonally-arranged electrode array, where each active electrode is surrounded by six guards, which collectively return the stimulus current (Hex electrodes). This array design is advantageous in that it isolates each active electrode from neighboring active electrodes and therefore confines the stimulus current to a small area around the center electrode and minimizes electrode cross-talk [6-8].

In retinal implants, electrical stimulus pulses delivered via the electrode array evoke action potentials in retinal ganglion cells (RGCs). Electrical stimulation activates the RGCs either directly or indirectly. Indirect RGC activation results from excitation of retinal neurons that provide synaptic input to RGCs. It is still unknown whether direct or synaptic RGC stimulation is the more suitable approach for retinal implants. Because of the extensive remodeling that occurs in retinal degenerative diseases [9], it might be advantageous to target ganglion cells directly, bypassing the compromised retinal circuitry. Moreover, unlike synaptic responses, direct RGC responses are possible to elicit using high stimulus frequencies and with high temporal precision [10]. The drawback of direct RGC stimulation, however, is activation of the axons in the nerve fiber layer, which have somas located far from the stimulating electrodes. If these axons are excited, the brain might interpret the signals as responses originated at distant somas of these cells, and possibly result in elongated percepts, reducing the quality of the perceived images.

A number of RGC types are present in the retina. In the central region of human and primate retinas, midget cells are the most numerous, making up 95% of all ganglion cells [11]. These cells are characterized by small dendritic trees and are perhaps the homologues of the beta cells in the cat retina [12, 13]. Due to their small size and large population, it is likely that the vast majority of the RGCs stimulated with retinal electrodes belong to this group.

In the present study a computational model of electrical stimulation of a cat beta RGC with epiretinal Hex electrodes was employed in order to obtain an activation threshold map.

II. Methods

Computational model of a beta RGC activation

A 3D computational model of electrical stimulation of a cat beta RGC, based on the formulation by Fohlmeister et al. [14], was implemented in COMSOL Multiphysics 4.1 software (COMSOL AB, Sweden).

The model geometry consisted of a 500 x 500 x 35 μm^3 conductive volume , representing the RGC layer , and a ganglion cell placed below the retinal surface. The cell geometry consisted of one-dimensional edges representing

M. Abramian, S. Dokos, G.J. Suaning and N.H. Lovell are with the Graduate School of Biomedical Engineering. The University of New South Wales, Sydney, Australia. J.W. Morley is with the School of Medicine, University of Western Sydney, Campbelltown, Australia.

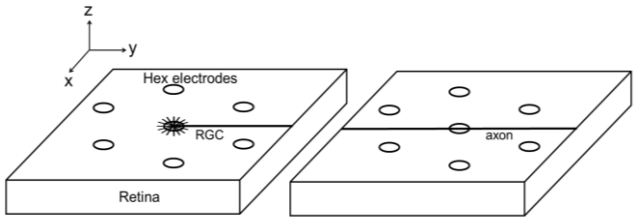

Figure 1. Model geometry (not to scale). RGC layer was modeled as a conductive block. Disk electrodes placed on the retinal surface were used for simulated electrical stimulation. Left: an RGC consisting of dendrites, soma and axon was located below the retinal surface. Right: the cell geometry consisted only of the distal axon.

the dendrites, the soma and the axon (Figure 1). The dendritic tree consisted of 24 branches, originating from the soma. The axon was comprised of three sections: the initial segment (IS), the trigger segment (TS) and the distal axon. The axon and the dendritic tree were located 0.5 and 1.5 μm below the retinal surface, respectively. Lengths and diameters of the cell elements were chosen based on morphological data of the cat beta RGCs reported by Fohlmeister et al [14]. Dimensions and ionic conductances of each cell element are shown in Table 1. In some simulations, the model geometry only consisted of the distal axon. This axon-only model represented cells whose somas were a long distance from the electrodes.

Simulated electrical stimulation was delivered via seven disks forming a Hex electrode on the retinal surface. Electrodes tested were 10 or 50 μm in diameter, with center-to-center spacing of 200 μm. Stimulus signals were 100 μs/phase anodic-first biphasic current pulses, which were delivered at the Hex center and one sixth of the total current was returned at each of the surrounding electrodes.

Extracellular voltage (V_e) distribution was governed by

$$\sigma_e \nabla^2 V_e = -I_m \tag{1}$$

where σ_e is the extracellular conductivity and I_m is the RGC membrane current density per unit volume, given by

$$I_m = \frac{2}{r}\left(C_m \frac{\partial V_m}{\partial t} + J_{ion}\right) = \sigma_i \frac{\partial^2 V_i}{\partial s^2} \tag{2}$$

where r is the radius of each cell element (Table 1), C_m is the membrane capacitance, V_m is the transmembrane potential and J_{ion} is the total ionic current per unit membrane area, given by

$$V_m = V_i - V_e \tag{3}$$

$$J_{ion} = \overbrace{g_{Na} m^3 h (V_m - V_{Na})}^{i_{Na}} + \overbrace{g_{Ca} c^3 (V_m - V_{Ca})}^{i_{Ca}} + \overbrace{g_K n^4 (V_m - V_K)}^{i_K} + \overbrace{g_A a^3 h_A (V_m - V_K)}^{i_{Ka}} + \overbrace{g_{K,Ca} (V_m - V_K)}^{i_{KCa}} + \overbrace{g_L (V_m - V_L)}^{i_L} \tag{4}$$

Here, g terms are the membrane conductances for the ionic currents (Table 1 and 2), and m, n, h, c, a, h_A are gating variables governed by first-order kinetics:

$$\frac{dx}{dt} = \alpha_x (1-x) - \beta_x x \tag{5}$$
$$x \equiv m, n, h, c, a, h_A$$

where α_x and β_x rate constants are functions of transmembrane potential V_m [14].

The reversal potential for calcium current was given by

$$V_{Ca} = \frac{RT}{2F} \ln\left(\frac{[Ca]_e}{[Ca]_i}\right) \tag{6}$$

and the intracellular calcium concentration was governed by first-order kinetics:

$$\frac{d[Ca]_i}{dt} = \frac{-3 I_{Ca}}{2F\lambda_r} - \frac{([Ca]_i - [Ca]_{res})}{\tau_{Ca}} \tag{7}$$

where, $[Ca]_{res}$ is the resting cytosolic calcium concentration, τ_{Ca} is the calcium removal time constant and λ_r is the calcium buffer volume to surface ratio.

On all external boundaries, except for the electrodes and the two walls of the retina which run parallel to the RGC, zero flux boundary condition was applied. Those two walls were set to ground.

Conductivity of the RGC layer was set to 0.9 S/m, to replicate in vitro average threshold values obtained for rabbit RGCs, using the same electrode and stimulus parameters [15]. This conductivity value is comparable with physiological conductivities obtained in the rat retina [16]. All other parameters were those reported by Fohlmeister et al. [14] (Table 2).

To obtain threshold maps, the Hex electrodes were moved laterally relative to the cell, in 100 μm increments, and RGC activation threshold was measured at each point. For each threshold measurement, a range of current amplitudes was tested and two consecutive pulses (with a typical amplitude difference of 10%) were found, where the higher amplitude evoked an action potential but the lower amplitude did not evoke a response. Threshold was defined as the average of those two amplitude values.

III. Results

A. Beta RGC activation thresholds as a function of Hex electrode size

When the stimulus pulse was delivered via the Hex electrodes, the cell membrane was depolarized. If the current amplitude was supra-threshold, an action potential was initiated and propagated down the axon. If the current amplitude was sub-threshold, the membrane potential returned to its resting value of -70 mV.

With 50 μm electrodes and 100 μs/phase pulse duration, TS (y=100 μm) and axonal (y= 200 μm) activation thresholds were 4.7 and 4.9 μA, respectively; whereas with 10 μm electrodes, these thresholds were 0.67 and 1.12 μA. These thresholds correspond to charge densities of 24 and 25 μC/cm^2 for 50 μm electrodes and, 85 and 143 μC/cm^2 for 10 μm electrodes.

	Soma	Dendrites	IS	TS	DA
Diameter	10	0.6	1	0.6	1
Length	10	40	45	90	355
g_{Na}	69.4	63.9	100	244.5	124
g_K	32	13.4	50.1	50.1	50
g_{Ca}	1.39	1.39	0.836	0	4

Table. 1. Geometrical parameters (µm) and ionic conductances (mS/cm^2) of different RGC elements. IS: initial segment, TS: trigger segment, DA: distal axon.

Symbol	Description	Value	Units
σ_i	Intracellular conductivity	0.9	S/m
σ_e	Extracellular conductivity	0.9	S/m
C_m	RGC membrane capacitance	1	µF/cm²
g_A	Membrane conductance of i_{Ka}	54	mS/cm²
g_{KCa}	Membrane conductance of i_{KCa}	0.065	mS/cm²
V_{Na}	*Na* reversal potential	60.6	mV
V_K	*K* reversal potential	-101.34	mV
V_L	Leakage reversal potential	-64.58	mV
$[Ca]_{res}$	Resting cytosolic *Ca* concentration	0.1	µM
$[Ca]_e$	Extracellular *Ca* concentration	2	mM
τ_{Ca}	*Ca* removal time constant	1.5	ms
λ_r	*Ca* buffer volume to surface ratio	600	nL/cm²
F	Faraday constant	96.48	C/mmol
R	Universal gas constant	8.31	J/mol.K
T	Absolute temperature	310	K

Table. 2. Model parameters. All parameters were those reported by Fohlmeister et al. [14], except for intracellular and extracellular conductivities, which were chosen based on in vitro data (see Methods).

B. Spatial pattern of the Beta RGC activation

Activation thresholds of the RGC were measured and a total of 42 threshold values were used to obtain contour plots for activation near the cell body as well as the distal axon. The maximum current amplitude tested was 400 µA. Where this amplitude failed to evoke an action potential, the threshold for that point was taken to be 400 µA.

The threshold map showed that the neural activation pattern was asymmetric and greatly dominated by the axonal excitation. While activation was effectively contained within the Hex in the region beyond the soma (Figure 2, the left-half of the RGC threshold plot), an elongated activation shape was observed along the axon (Figure 2, the right-half of the RGC threshold plot). Activation map of the distal axon was identical to that of the proximal axon, 200 µm away from the soma (Figure 2).

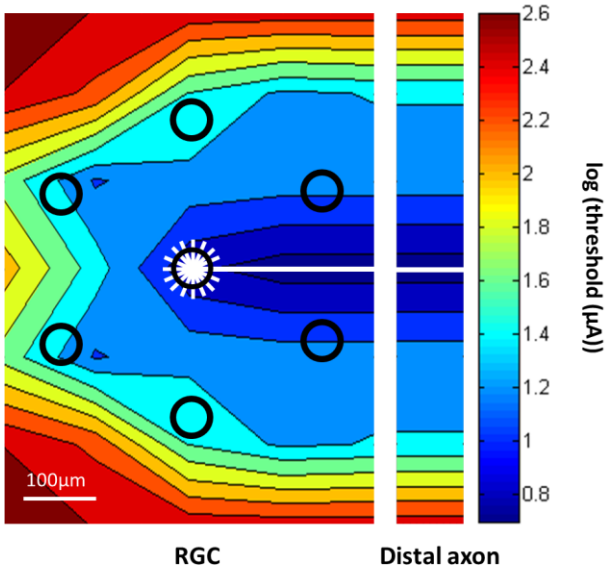

Fig. 2. Contour map of a beta RGC activation thresholds following electrical stimulation with 50 µm Hex electrodes. The color bar indicates log(threshold(µA)). Left: activation pattern in the vicinity of the cell body. Right: activation pattern of the distal axon. To obtain activation thresholds for the distal axon, the model geometry only consisted of the distal axon (Figure 1). Black circles show the position of the Hex electrodes. White lines indicate the RGC.

IV. Discussion

In agreement with previous studies, threshold charge was lower but threshold charge density was higher for smaller electrodes [15, 17-19]. Assuming a safe charge density limit of 100 µC/cm^2 for platinum electrodes [20], the model predicts that the electrode diameter can be safely reduced to 10 µm.

When RGCs are activated directly, the action potential initiation site is known to be the high sodium channel density region in the proximal axon [21, 22]. In this study, in the case of the smaller electrodes, TS (which is the high sodium channel density region) was 1.7 times more excitable than the distal axon. In contrast, there was almost no difference between the activation thresholds of these two regions when stimulating electrodes were relatively large.

In a similar modeling study, Greenberg et al. [23] investigated amphibian RGC stimulation with monopolar point source and disk electrodes. They reported that with point source stimulation, axonal excitation threshold was 1.73 times higher than the threshold near the soma. On the other hand, using 50 µm diameter disk electrodes and a Hodgkin-Huxley model they found that the axonal threshold was 20% higher than threshold for activation near the soma. This threshold difference was greater than the 4% difference found in the present study, possibly due to the fact that a different ionic model was used.

In contrast to our findings, Jensen et al. [19] investigated in vitro rabbit retinal stimulation and found that threshold for near soma stimulation was 3-4 times lower than that for the axons. The difference between these findings can be due in

part to the difference in RGC types: Jensen et al. studied brisk transient (alpha) cells in peripheral retina of the rabbit. These are the largest RGCs and their morphological properties differ considerably from those of the beta cell in the present study. Moreover, their electrode configuration was monopolar trans-retinal, resulting in significantly different electric fields compared to the Hex electrodes.

The activation map of the distal axon was identical to that of the proximal axon, 200 μm away from the soma, suggesting that at 200 μm distance, soma, dendrites, IS and TS had little or no influence on the axonal activation threshold.

V. Conclusion

Simulated epiretinal stimulation of a cat beta RGC showed that following stimulation with hexagonally arranged epiretinal electrodes the threshold profile had an elongated shape due to the low threshold of the axon. Axonal activation is a concern for retinal implant design and it is crucial to explore suitable stimulation strategies in order to minimize their excitation.

Many factors are likely to affect the spatial patterns of RGC activation, including: cell properties, size and configuration of the stimulating electrodes, as well as stimulus waveform parameters. The aim of our ongoing research is to use the computational model presented here to study spatial profiles of RGC activation, as a function of cell and stimulus parameters. The results can be useful in finding the optimum set of stimulus parameters that will induce a desired retinal activation pattern using a prosthetic device.

Acknowledgment

This research was supported by the Australian Research Council through its Special Research Initiative in Bionic Vision Science and Technology grant to Bionic Vision Australia.

References

[1] T. Guenther, N. H. Lovell, and G. J. Suaning, "Bionic vision: system architectures: a review," *Expert Rev Med Devices*, vol. 9, pp. 33-48, 2012.

[2] S. H. Greenwald, A. Horsager, M. S. Humayun, R. J. Greenberg, M. J. McMahon, and I. Fine, "Brightness as a function of current amplitude in human retinal electrical stimulation," *Invest Ophthalmol Vis Sci*, vol. 50, pp. 5017-25, 2009.

[3] J. F. Rizzo III, J. Wyatt, J. Loewenstein, S. Kelly, and D. Shire, "Perceptual efficacy of electrical stimulation of human retina with a microelectrode array during short-term surgical trials," *Invest Ophthalmol Vis Sci*, vol. 44, pp. 5362-5369, 2003.

[4] K. Cha, K. W. Horch, and R. A. Normann, "Mobility performance with a pixelized vision system," *Vision Res*, vol. 32, pp. 1367–1372, 1992.

[5] M. S. Humayun, E. de Juan, Jr., J. D. Weiland, G. Dagnelie, S. Katona, R. Greenberg, and S. Suzuki, "Pattern electrical stimulation of the human retina," *Vision Res*, vol. 39, pp. 2569-2576, 1999.

[6] N. H. Lovell, S. Dokos, S. C. Cloherty, P. Preston, and G. J. Suaning, "Current distribution during parallel stimulation: Implications for an epiretinal neuroprosthesis," *Conf Proc IEEE Eng Med Biol Soc*, vol. 5, pp. 5242 - 5245, 2005.

[7] N. B. Dommel, Y. T. Wong, T. Lehmann, C. W. Dodds, N. H. Lovell, and G. J. Suaning, "A CMOS retinal neurostimulator capable of focussed, simultaneous stimulation," *J Neural Eng*, vol. 6, pp. 035006, 2009.

[8] Y. T. Wong, N. Dommel, P. Preston, L. E. Hallum, T. Lehmann, N. H. Lovell, and G. J. Suaning, "Retinal neurostimulator for a multifocal vision prosthesis," *IEEE Trans Neural Syst Rehabil Eng*, vol. 15, pp. 425-434, 2007.

[9] R. E. Marc, B. W. Jones, C. B. Watt, and E. Strettoi, "Neural remodeling in retinal degeneration," *Prog Retin Eye Res*, vol. 22, pp. 607-655, 2003.

[10] S. I. Fried, H. A. Hsueh, and F. S. Werblin, "A method for generating precise temporal patterns of retinal spiking using prosthetic stimulation," *J Neurophysiol*, vol. 95, pp. 970-978, 2006.

[11] D. M. Dacey, "The mosaic of midget ganglion cells in the human retina," *J Neurosci*, vol. 13, pp. 5334-55, 1993.

[12] H. Wässle, "Parallel processing in the mammalian retina," *Nat Rev Neurosci*, vol. 5, pp. 747-757, 2004.

[13] H. Wässle, B. B. Boycott, and R. B. Illing, "Morphology and mosaic of on- and off-beta cells in the cat retina and some functional considerations," *Proc R Soc Lond B Biol Sci*, vol. 212, pp. 177-95, 1981.

[14] J. F. Fohlmeister, E. D. Cohen, and E. A. Newman, "Mechanisms and distribution of ion channels in retinal ganglion cells: using temperature as an independent variable," *J Neurophysiol*, vol. 103, pp. 1357-1374, 2010.

[15] M. Abramian, N. H. Lovell, J. W. Morley, G. J. Suaning, and S. Dokos, "Activation of retinal ganglion cells following epiretinal electrical stimulation with hexagonally arranged bipolar electrodes," *Journal of Neural Engineering*, vol. 8, 035004, 2011.

[16] H. Kasi, R. Meissner, A. Babalian, H. van Lintel, A. Bertsch, and P. Renaud, "Direct localised measurement of electrical resistivity profile in rat and embryonic chick retinas using a microprobe," *Journal of Electrical Bioimpedance* vol. 1, pp. 84-92, 2010.

[17] C. Sekirnjak, P. Hottowy, A. Sher, W. Dabrowski, A. M. Litke, and E. J. Chichilnisky, "Electrical stimulation of mammalian retinal ganglion cells with multielectrode arrays," *J Neurophysiol*, vol. 95, pp. 3311-3327, 2006.

[18] A. K. Ahuja, M. R. Behrend, M. Kuroda, M. S. Humayun, and J. D. Weiland, "An in vitro model of a retinal prosthesis," *IEEE Trans Biomed Eng*, vol. 55, pp. 1744-1753, 2008.

[19] R. J. Jensen, O. R. Ziv, and J. F. Rizzo, 3rd, "Thresholds for activation of rabbit retinal ganglion cells with relatively large, extracellular microelectrodes," *Invest Ophthalmol Vis Sci*, vol. 46, pp. 1486-1496, 2005.

[20] T. L. Rose and L. S. Robblee, "Electrical stimulation with Pt electrodes. Vlll. Electrochemically safe charge injection limits with 0.2ms pulses," *IEEE Trans Biomed Eng*, vol. 37, pp. 1118-1120, 1990.

[21] S. I. Fried, A. C. Lasker, N. J. Desai, D. K. Eddington, and J. F. Rizzo, 3rd, "Axonal sodium-channel bands shape the response to electric stimulation in retinal ganglion cells," *J Neurophysiol*, vol. 101, pp. 1972-1987, 2009.

[22] C. Sekirnjak, P. Hottowy, A. Sher, W. Dabrowski, A. M. Litke, and E. J. Chichilnisky, "High-resolution electrical stimulation of primate retina for epiretinal implant design," *J Neurosci*, vol. 28, pp. 4446-4456, 2008.

[23] R. J. Greenberg, T. J. Velte, M. S. Humayun, G. N. Scarlatis, and E. de Juan, Jr., "A computational model of electrical stimulation of the retinal ganglion cell," *IEEE Trans Biomed Eng*, vol. 46, pp. 505-514, 1999.